Petrography and geochemistry of the magnesites and dolostones of the Ediacaran Ibor Group (635 to 542 Ma), Western Spain: Evidences of their hydrothermal origin

M.J. Herrero [a,*], Andrea Martín-Pérez [a], Ana M. Alonso-Zarza [a,d], Inma Gil-Peña [b], Alfonso Meléndez [c], Rebeca Martín-García [a,d]

[a] Dept. of Petrology and Geochemistry, Faculty of Geological Sciences, Universidad Complutense de Madrid-CSIC, 28040 Madrid, Spain
[b] Instituto Geológico y Minero de España (IGME), Río Rosas 23, 28003 Madrid, Spain
[c] Dept. of Earth Sciences, Faculty of Science, Universidad de Zaragoza, 50009 Zaragoza, Spain
[d] Instituto de Geociencias (UCM-CSIC), C/José Antonio Novais, 28040 Madrid, Spain

Keywords:
Dolostones
Magnesites
Hydrothermal
Burial
Replacement
Ediacaran

A B S T R A C T

The Ediacaran deposits (between 635 and 542 Ma) of the Central Zone of the Iberian Massif consist of alternating siliciclastic and carbonate beds. These carbonates are dolostones and magnesites which are interpreted to have been formed by the replacement of primary peritidal limestones. Through petrographic and geochemical analyses, we recognize different types of dolomites (D1 to D4) and magnesites (M1 and M2). Despite distinct petrographic features of the four types of dolomite, their oxygen and carbon isotopes overlap with $\delta^{18}O$ values ranging from +15.45 to +17.51‰ (SMOW) and $\delta^{13}C$ from −0.13 to 3.21‰ PDB. Sr isotope values for D1 and D2 range from 0.7028 to 0.7091. Magnesites (M1 and M2) show oxygen values higher than +17.87.0‰, and $\delta^{13}C$ values show the same variability as for the dolomites. D3 and D4 oxygen isotope values are between +18.91 and 19.61, and the carbon isotope values range are similar to the other diagenetic phases. Sr isotope values for the magnesites and late dolomites (D3 and D4) are 0.7095 to 0.7104, being higher than those of the D1 and D2 dolomites. D1 is a relatively early dolomite phase formed by the replacement of fine grained peritidal limestones. The coarser crystal size of D2, which shows similar geochemical features as D1, suggests formation by dolomitization of coarser grained limestones. The replacement of D1 and D2 by M1 and M2 advanced along stylolites, fractures and bedding planes. This replacement is interpreted to have occurred by hydrothermal fluids, which is suggested by the presence of talc and forsterite. D3, a coarse dolomite, completely destroyed any previous texture and D4 (dolomite cement) post-dates magnesite formation. Interactions of hydrothermal fluids with the prior carbonates reset the oxygen isotopes of the earlier dolomite.

The study of these magnesites and related dolostones may offer new insights into the model of formation of sparry magnesites hosted by mixed siliciclastic–carbonate platform deposits. The establishment of the factors and mechanism that control the diagenetic evolution of these carbonates has a great importance in order to understand and predicts porosity and permeability variations of rocks formed under similar geological conditions.

1. Introduction

Although it is not well understood how the Mg-rich carbonates of the Ibor Group formed, they have attracted the attention of researchers because: a) they are among the oldest carbonates preserved in the Iberian Peninsula, b) they contain fossils of the first metazoans bearing a carbonate exoskeleton (Cortijo et al., 2010) and, c) they record a complex diagenetic history which may be useful to understand the mechanisms that gave rise to other similar, though rare, magnesian carbonate deposits.

Magnesite appears in modern coastal and continental environments (Pueyo and Inglés, 1987; Schroll, 2002) as well as in ancient sedimentary sequences (Zachmann, 1989). When formed in sedimentary conditions, magnesite is always considered a secondary carbonate and typical product of advanced diagenesis (Müller et al., 1972). Pohl (1990) distinguished two types of economically important magnesite deposits: 1) cryptocrystalline magnesites with Mg sourced by ultramafic magmatic host rocks (Pohl, 1989), and 2) stratabound lenses of coarse crystalline magnesites which are associated with marine platform environments such as those examined in this paper. The origin of the second type of magnesite is controversial and there are two main models for its formation. In the first model, magnesite is considered to be a product of synsedimentary processes related to evaporitic conditions or to early diagenetic transformations

* Corresponding author.
E-mail address: mjherrer@pdi.ucm.es (M.J. Herrero).

of carbonates (Pohl, 1990; Melezhik et al., 2001). Magnesite precipitation has been suggested to occur in evaporitic sabkha-type environments (Quemeneur, 1974) or from Mg-concentrated brines originated by early diagenetic compaction of clays (Siegl, 1984). The second model considers an epigenetic origin, which involves hydrothermal/metasomatic replacement of dolostones during thermal events (Dulski and Morteany, 1989; Zachmann and Johannes, 1989; Lugli et al., 2000; Machel and Lonnee, 2002; Kilias et al., 2006).

In this paper, we discuss the origin of the magnesites and dolostones of the Upper Proterozoic (Ediacaran) deposits of the Ibor Group (Liñán et al., 2002). Sedimentology, petrology, diagenesis and geochemistry analyses permit to establish a dataset that characterizes magnesite deposits formed under hydrothermal conditions. This model is useful to understand the genesis of similar magnesian deposits in other parts of the world and offers an alternative explanation for magnesite deposits that have been interpreted as the result of evaporation processes.

2. Geological setting

The Ediacaran–Lower Cambrian Ibor Group crops out in the easternmost area of the Central Iberian Zone of the Iberian Massif. This area is characterized by extensive exposure of low grade to unmetamorphosed sedimentary series of the Ediacaran–Lower Cambrian Schist–Greywacke complex (Fig. 1).

The Schist–Greywacke complex can be subdivided into two large stratigraphic units, the Domo Extremeño Group and the Ibor Group (Alvarez-Nava et al., 1988; Valladares et al., 1993) separated by a sedimentary discontinuity (Valladares et al., 2000, 2002; Rodríguez-Alonso et al., 2004). The Domo Extremeño Group consists of a thick and monotonous succession of shales, sandstones and greywackes. The Ibor Group consists of an alternation of shales, sandstones and greywackes (Fig. 2), with intercalations of decimetre to meter thick carbonate levels (dolostones and magnesites) deposited on a mixed carbonate–siliciclastic platform (Palacios Medrano, 2005). In the Ibor area, these carbonates preserve remains of *Cloudina hartmannae* suggesting a latest Ediacaran age no older than 560 Ma (Vidal et al., 1994b). Phanerozoic-appearing trace fossils (Liñán et al., 2002 and references therein) and Early Cambrian fossils (trilobites, the mollusc *Anabarella* and age-diagnostic acritarchs) have been found above the *Cloudina*-bearing carbonates in the terminal levels of the Ibor Group (Vidal et al., 1999). Evidence of reworking and resedimentation of the uppermost Ediacaran carbonate platform during Lower Cambrian times has been reported for eastern and northwestern areas of the Central Iberian Zone (Vidal et al., 1994b; Valladares et al., 2000, 2002). The upper part of the Lower Cambrian succession is absent in the area.

The outcrops examined appear in the Ibor Antiform, a Variscan large-scale vertical fold that defines the Domain of Vertical Folds (Díez-Balda et al., 1990). This fold has a N150E trend (Fig. 1) and shows a general box fold geometry slightly verging to the SW. Wide anticlines cored in the Neoproterozoic deposits are separated by narrow synclines delineated by the Armorican Quartzite. Syn- to late Variscan granites cut across these structures.

Ediacaran carbonate units reproduce this fold geometry on a decametric scale. Superimposed on the folding structure are longitudinal and transverse fault and fracture systems. Main faults are sinistral-normal faults trending ESE to E–W, conjugated with secondary NE to NNE faults. NW faults are typically associated with the hinge areas of the folds. Minor fractures reproduce similar orientations and also present a N060E joint set.

These features are the result of complex tectonic evolution throughout the Cadomian, Variscan and Alpine cycles. Evolution through the Ediacaran–Variscan time span gave rise to various tectonic signatures in the Ibor area. There are no clear reflections of metamorphism or internal strain related to the Ediacaran–earliest Cambrian Cadomian tectonic events (Díez-Balda et al., 1990). Instead, the basal early Cambrian erosional surface is attributed to a relative sea-level fall (Valladares et al., 2000). Subaerial exposure produced intense weathering of the Ediacaran–Cambrian boundary materials (Valladares et al., 2000, 2002). The upper part of the Lower Cambrian sequence is absent in the area as a consequence of the thermal expansion, tilting, uplift and erosion suffered by the succession during the main episode of rift-related activity in the adjacent Ossa Morena Zone (López-Guijarro et al., 2008 and references therein). This event produced intense erosion of the upper Cambrian sequence and the resultant unconformity (sardic unconformity (Lotze, 1956)) appears overlaid by a transgressive Ordovician–Devonian sequence formed in a passive margin setting. A generalized transgressive event in the Central Iberian Zone led to the deposition of Armorican Quartzite, which is a continuous Ordovician to Lower Carboniferous sedimentation record of siliciclastic marine platforms developed at the Gondwana margins of a passive continental margin.

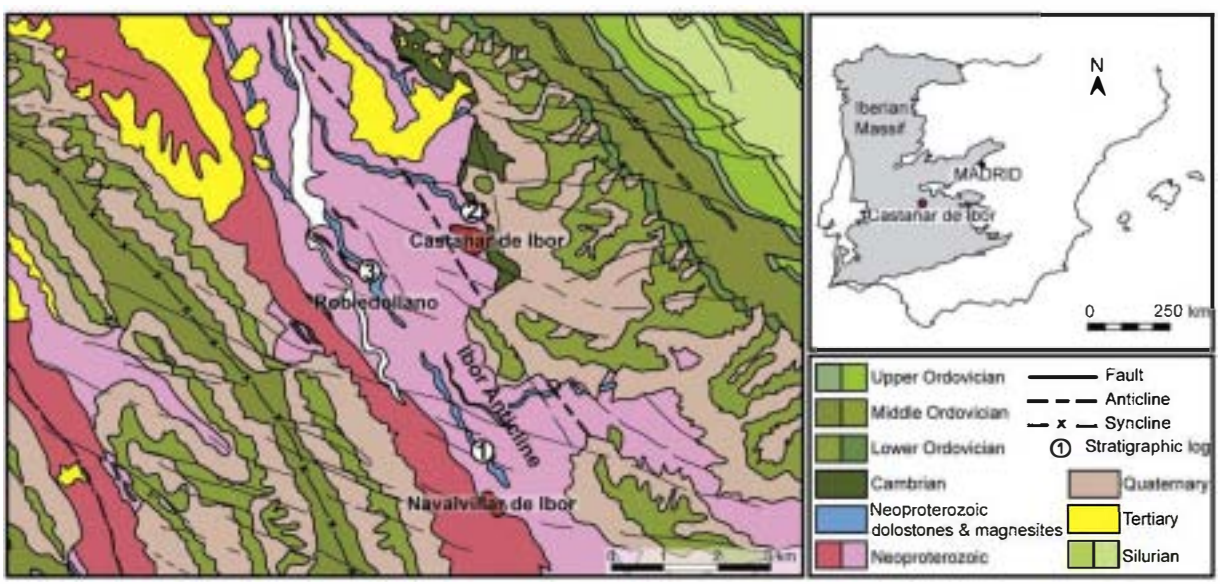

Fig. 1. Geologic map of the study area. The sections examined were from: 1) Navalvillar, 2) Castañar, and 3) Robledollano.

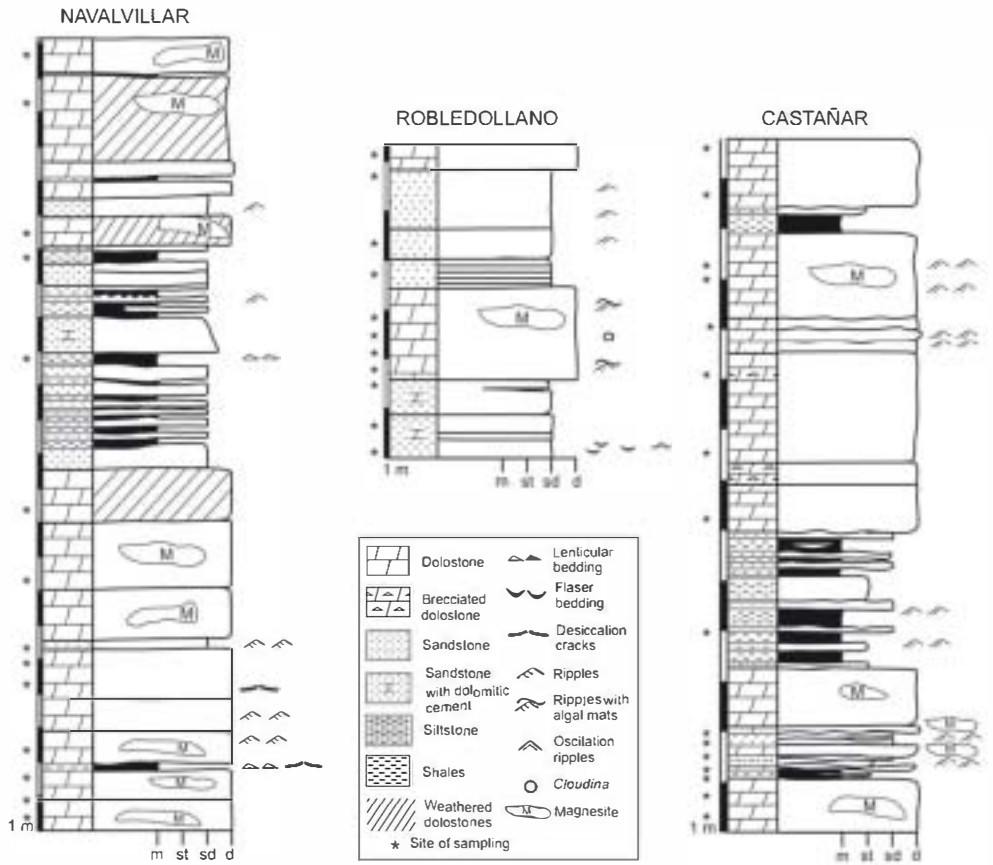

Fig. 2. Logs of the Navalvillar, Robledollano and Castañar sections. Note that these all correspond to deposits of the Ibor Group.

During the Carboniferous, the Variscan orogeny promoted intense deformation, regional metamorphism and massive granite intrusion in the study area. This Variscan deformation is responsible for the vertical folds (Ibor antiform), the NW faults associated with the hinge area of the folds, and the cleavage found in Neoproterozoic–Silurian sequences. Metamorphism in this area was only very low grade or anchymetamorphism.

Late Variscan calc-alkaline granitoid bodies showing weak internal deformation appear widely distributed in the Central Iberian Zone, with emplacement ages ascribed of between 330 and 285 Ma. (Villaseca et al., 1995). These bodies cut across the Ibor anticline, giving rise to a 1 km wide metamorphic aureole in the uppermost Ediacaran and Ordovician–Silurian host rocks (IGME, 1978; 1983). Later, the batholite was fractured by the Alentejo–Plasencia Fault. This tectonic feature, active from last-Variscan times to the present day (Villamor-Pérez, 2002), bounds to the NW the vertical folds of the Ibor area and records a Jurassic thermal event (Dunn et al., 1998).

The Alpine evolution of this area also includes uplifting and progressive exhumation of the Variscan basement in the Mesozoic, subsidence of the adjacent Tajo Basin during the Tertiary and gradual dissection by the fluvial network.

3. Methods

Conventional petrography analyses were performed on 54 thin sections stained with alizarin red S to differentiate calcite from other carbonate minerals. Scanning electron microscopy (SEM) observations were made on gold-coated samples using a JEOL 6400 electron microscope working at 20 kV and with a resolution of 35 Å. Secondary electron and backscattering detectors were used together with an X-ray detector system to obtain semiquantitative compositions. The Ca, Mg, Fe, Sr, and Mn contents of the different minerals in selected polished samples were obtained using an electron microprobe (JEOL JXA 8900 M) operating at 15 kV and 20 nA and employing an electron beam diameter of 5 μm. The standards used are described by Jarosewich et al. (1980) and were provided by the Smithsonian Institute, Washington, USA. Powdered samples were mineralogically characterized using a Philips PW-1710 X-ray diffraction (XRD) system operating at 40 kV and 30 mA, and employing monochromated CuKα radiation. XRD spectra were obtained from 2 to 66° 2θ. The $\delta^{13}C$ and $\delta^{18}O$ values of 25 powdered samples were later analyzed at the Stable Isotope Laboratory, Salamanca University. The fractioned extraction of CO_2 from carbonates to perform C and O isotope analyses was conducted using standard techniques (Craig, 1957). Samples were powdered and allowed to react with 100% phosphoric acid at 25° for at least 72 h. The gas emitted in this time span was attributed to dolomite, whereas for magnesite the time of analysis was approximately 10 days. The experimental error for carbonates ($\delta^{13}C$ and $\delta^{18}O$) was ± 0.1‰ for carbon and ± 0.15‰ for oxygen. Oxygen values are reported relative to standard mean ocean water (SMOW) whereas carbon values are reported in δ ‰ relative to PDB. In order to correct temperature-dependent fractionation between carbonates and phosphoric acid, values of 2.03‰ and 0.83‰ were subtracted from magnesite and dolomites values respectively (Lugli et al., 2002). The dolomite–water fractionation factor has been obtained by a combination of the calcite–water fractionation factor of O'Neil et al. (1969) and the dolomite–calcite fractionation factor of Sheppard and Schwarcz (1970). For the magnesite–water oxygen isotope fractionation factor we have used the one from Aharon (1988). For carbon, the dolomite–CO_2 fractionation factor of Ohmoto and Rye (1979) was based on the dolomite–calcite fractionation factor given by Sheppard and Schwarcz (1970). Between magnesite and CO_2 the fractionation factor has been approximated to that of the dolomite–CO_2 (Aharon, 1988; Lugli et al., 2002).

Six samples were selected for radiogenic $^{87}Sr/^{86}Sr$ isotope analysis performed at the Geochronology and Isotope Geochemistry facility of the Universidad Complutense de Madrid using a VG TIMS mass spectrometer. A small-drill (0.5 mm in diameter) was used to avoid mixing of the different minerals. The samples were dissolved in 2.5 N HCL, centrifuged and then evaporated. The residue was again dissolved in 2.5 N HCL. The analytical precision for $^{87}Sr/^{86}Sr$ analysis is 0.01‰.

4. Sedimentology

The magnesites and dolostones examined here appear in three units at the top of the Ibor Group. The lower unit was studied in the Robledollano and Navalvillar sections and the middle one in the Castañar section (Fig. 2). The upper unit does not crop out in good conditions. Carbonate units (dolostones and magnesites) are up to 10 m thick and are separated by intercalations of detrital beds of sandstones and shales (Fig. 3A). In the field, dolostones are gray in color whereas magnesites appear brownish. The three carbonate units show similar features although most of their primary structures and textures have been erased by dolomitization and/or magnesitization processes.

1) Dolostones appear as both massive and laminated. Massive dolostones occur in bodies more than 1 m thick (Fig. 3A). These bodies consist of a coarse mosaic of dolomite including ghosts of *Cloudina hartmannae* (Figs. 2 and 4A, Robledollano section), which is considered the first metazoan with a mineralized exoskeleton (Vidal et al., 1994a; Cortijo et al., 2010). Some detrital quartz grains are also found in the massive dolostones. Laminated dolostones show parallel lamination, ripple-cross, lenticular and flaser beddings and flat-pebble breccia at their tops (Fig. 3B). The arrangement of sedimentary structures is similar to that commonly found in the shallowing-upwards tidal sequences of carbonate platforms (Walker and Plint, 1992). In addition, there are undulated laminations that have been interpreted as stromatolic laminations (Palacios Medrano, 2005) also confirming the shallow nature of the depositional environment.
2) Siliciclastic deposits formed by thin (cm–dm) alternations of sandstones (greywackes) and shales (Fig. 3C). According to the geometry and internal structure of the decimetre-scale sandstone bodies, three types of sandstone deposit can be defined: a) sandstone bodies with flat bases and convex tops (lobes), b) sandstone bodies with channelized-like geometries such as scour and fill structures, and c) sandstone bodies of bar morphology showing

Fig. 3. A) Siliciclastic beds overlaid by carbonate bodies. B) Dolostones showing parallel lamination, lenticular and flaser beddings and flat-pebble breccia. C) Microphotograph of a shale sample showing abundant quartz grains and clay minerals concentrated in layers. D) Microphotograph of a greywacke containing chlorite grains. E) Dolostone beds interbedded within siliciclastic beds (greywackes and shales). F) Magnesitization front advancing through joints and fractures.

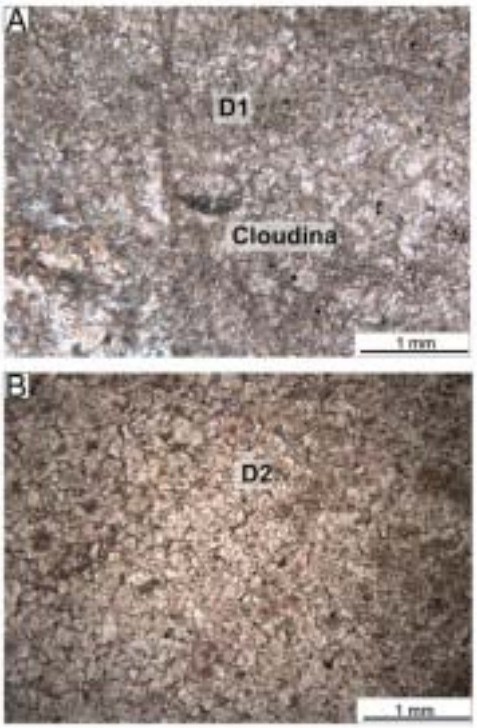

Fig. 4. Microphotographs: A) Dolomite 1 (D1): mosaic of Fe-rich dolomite crystals with *Cloudina* ghosts. B) Dolomite 2 (D2): mosaic of idiomorphic to subidiomorphic crystals.

cross-bedding. Thin sandstone beds also exhibit ripple cross bedding and flaser and lenticular bedding. Other sedimentary structures recognized are current and oscillation ripples and desiccation cracks. These thin sandstone beds are interbedded with shales, which appear in levels ranging from only a few mm to up to 10 cm thick and are dark gray to black in color. They are composed of clay minerals and quartz, with smaller amounts of plagioclase and K-feldspar (Fig. 3C). Clay minerals are mainly illite, chlorite, smectite and kaolinite. In some levels it is possible to find pyrite. In greywackes, grain size varies from very fine to medium, the mean size of the quartz grains being 0.15 mm. Grains are monocrystalline quartz and polycrystalline chert, plagioclase and K-feldspar (total feldspars from up to 10%) and trace amounts of tourmaline. They are classified as greywackes because they contain up to 40% of illite, chlorite, smectite and kaolinite matrix (Fig. 3D). Dolomitic cement is abundant and there are fractures filled with quartz cements.

The architectural facies arrangement is that characteristic of a mixed carbonate–siliciclastic platform environment (Palacios Medrano, 2005) which has been developed during Ediacaran times (IUGS, 2009). The depositional environment was characterized by tidal-flats (Vilas et al., 1987), where carbonate deposits would represent the shallower inter to supratidal facies, whereas the clastic deposits correspond to deeper and higher energy environments (subtidal) as described by Myrow and Landing (1992) in the Early Cambrian of Newfoundland. Similar well-preserved and thick sedimentary successions have been described at the Precambrian–Cambrian boundary in the Ara Group of Oman (Al-Husseini et al., 2003; Schröder et al., 2005), where carbonates alternate with evaporites. Le Guerroué et al. (2006) described a thick sedimentary succession, The Nafun Group, also in Oman, which show analogies to those identified in the Ibor Group.

5. Petrography

The dolostones and magnesites of the Ibor Group appear as carbonate bodies intercalated with the siliciclastic deposits already mentioned. The most cases dolomitization is pervasive but it mimics fossil and sedimentary structures. Magnesite replacement was not extensive and shows different features. In the Navalvillar section (Fig. 3E), magnesitization advanced through fractures and bedding planes; it was pervasive and in places totally replaced the dolostone. In the Castañar and Robledollano sections (Fig. 3F), replacement mostly advanced between the bedding planes and some primary sedimentary constituents are preserved. The dominant minerals include dolomite, magnesite, calcite, talc and forsterite.

5.1. Dolomite

Four different dolomite phases were distinguished (D1, D2, D3, and D4):

Dolomite 1 (D1) is characterized by non-planar, closely packed with subhedral crystals (0.1 to 0.3 mm) with undulatory extinction (Fig. 4A). The dolomite crystals are transparent to pale brown and cloudy, mainly due to the presence of abundant tiny fluid inclusions. Locally, the dolostones show ghosts of intraclasts and *Cloudina* (Fig. 4A) as well as some quartz grains.

Dolomite 2 (D2) consists of a mosaic of coarser, 0.1 to 1 mm size crystals. Most crystals are cloudy, appear unzoned in planar-light and mostly have planar crystal boundaries. The core of the crystals is brown, whereas overgrowth is less turbid (Fig. 4B). Differences in crystal size with respect to D1 are related to the original grain size of the sediments, since D1 replaces mud-dominated limestones, whereas D2 seems to replace packstone/grainstone limestones. D1 and D2 phases are cut by a network of stylolites (Fig. 5A, B), which do not show a net pattern and mostly show a high-amplitude distribution with a main set parallel to the stratification and a second set perpendicular to the former.

Dolomite 3 (D3). D3 dolomites show a coarser crystalline appearance than earlier dolomites. D3 consists of a mosaic of fine- to medium-grained (<1 mm) turbid crystals with poorly defined non-planar boundaries. The existence of an earlier dolomite precursor is possible but this cannot be determined given the obliteration of earlier textures (Fig. 5A).

Dolomite 4 (D4) appears as mm- to cm-sized crystals of dolomite as void-filling cement, clearer than the replacive crystals of dolomite D3 (Fig. 5C, D). The crystals show no zoning, curved crystal faces, with planar to undulating extinction and a sharp contact with other replacive phases. In outcrop it is observed that D4 is filling a series of boxwork vugs that appear aligned parallel to the main family of fractures. The vug distribution gives the rock a brecciated appearance (Fig. 5E, F).

5.2. Magnesite

Magnesite appears as two different diagenetic phases, M1 and M2. *Magnesite 1* (M1) is composed of unimodal, planar boundary crystals. Crystal size ranges from mm to cm. M1 is Fe-poor (Fig. 5B, C, D) and crystals. No relics exist of the previous texture of the rock. This magnesite initially occurs along stylolite, bedding and fracture planes (Fig. 6A), and ultimately totally replace the previous dolostone to form a massive body of magnesite.

Magnesite 2 (M2) is Fe-rich and banded, with goethite rims alternating with magnesite. The magnesite bands are about 0.8 mm whereas the goethite rims are very thin (0.1 mm). M2 occurs as overgrowths on M1 crystals and, in many cases, shows hexagonal sections (Fig. 6C). In some cases, the magnesite deposits show a brecciated appearance and boxwork vugs (Fig. 6B) aligned with joints and local fractures. Contact between the host rocks and magnesites is sharp. The stylolite surfaces present in the dolostones can be traced into the magnesite beds. No evaporite phase is associated with the magnesite crystals.

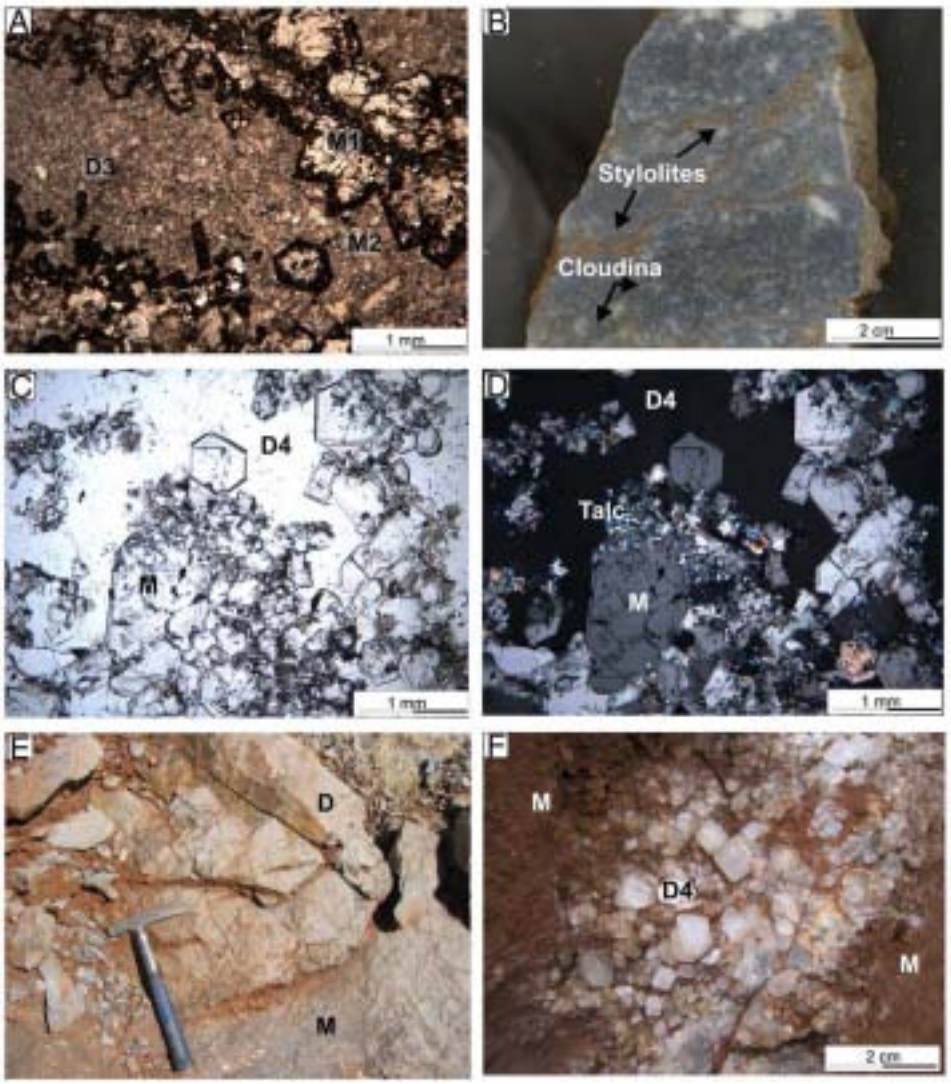

Fig. 5. A) Replacement advancing through fractures and bedding planes. Note the difference in color; the magnesite (M) appears darker and dolostone (D) lighter. B) Hand specimens of dolomites D1 and D2 that preserve the texture of previous *Cloudina* fossils and stylolites. C) Magnesite crystals (M) and dolomite cement (D4). D) Cross-polarized light images of the same sample as in E. Talc relations with magnesite crystals (M1) and dolomite cement (D4). E) Brecciated appearance of the magnesitization front. F) D4 dolomite crystals filling box work vugs.

5.3. Calcite

Low-Mg calcite appears as a late phase either replacing magnesite pseudomorphs or replacing dolomite. The magnesite (M1 and M2) pseudomorphs appear as planar calcite crystals (Fig. 7A, B). Calcitized dolomite and magnesite crystals are rich in Fe oxide inclusions (Fig. 6D).

5.4. Other diagenetic phases

Talc is associated with a second set of fractures within the magnesites and more commonly within the dolomites. Talc also appears in intercrystalline pores, forming small clusters or filling pockets within coarse sparry magnesite. The magnesite crystals are highly corroded in the vicinity of talc (Fig. 5F). Forsterite was only identified by SEM as 1 μm spheres (Fig. 8A) in pores, between magnesite or dolomite (D3 and D4) corroded crystals.

Goethite appears as thin rims between crystals of magnesite, especially of the M2 phase. Goethite occurs as acicular crystals coating both dolomite and magnesite or filling the porosity between crystals (Figs. 7A and 8B). Goethite is also abundant when the dolomite and magnesite crystals appear calcitized.

6. Geochemistry

6.1. Element composition

Average composition of CaO, MgO, FeO, SrO, and MnO was determined by microprobe analysis permit to characterize each of the phases (dolomites D1 to D4, magnesites M1 to M2 and C calcite) (Table 1). Concentration of Ca, Fe and Mg are plotted in Fig. 9.

D1 and D2 have rather similar composition, and both of these dolomites differ chemically form D3 and D4. D1 and D2 show high MgO (Fig. 10A) and low FeO contents (MgO ≈ 21.08 wt.% and FeO ≈ 0.98 wt.%) compared to D3 and D4 (MgO ≈ 20.00 wt.% and FeO ≈ 1.90 wt.%) (Fig. 10B). CaO contents ranging between 27.5 and 31.0 wt.% (Fig. 10C) and SrO contents up to 0.20 wt.% (Fig. 10D) are similar in all four phases. Electron microprobe analysis of the dolomite indicated similar Mn levels for the D1, D2 and D3 dolomites (between 0.12 and 0.16 wt.%). The two magnesite phases differ in that M1 has more MgO (43.00 wt.%) and less FeO (3.26 wt.%) and MnO (0.12 wt.%) than M2 (MgO ≈ 36.04 wt.%; FeO ≈ 14.91 wt.%; MnO ≈ 0.64 wt.%) (Fig. 11A, B), while CaO and SrO contents show similar variation in the two magnesite phases (CaO varies from 0.1 to 0.60 wt.% and Sr from 0.1 to 0.15 wt.%). In addition, M2 magnesite shows negative correlation

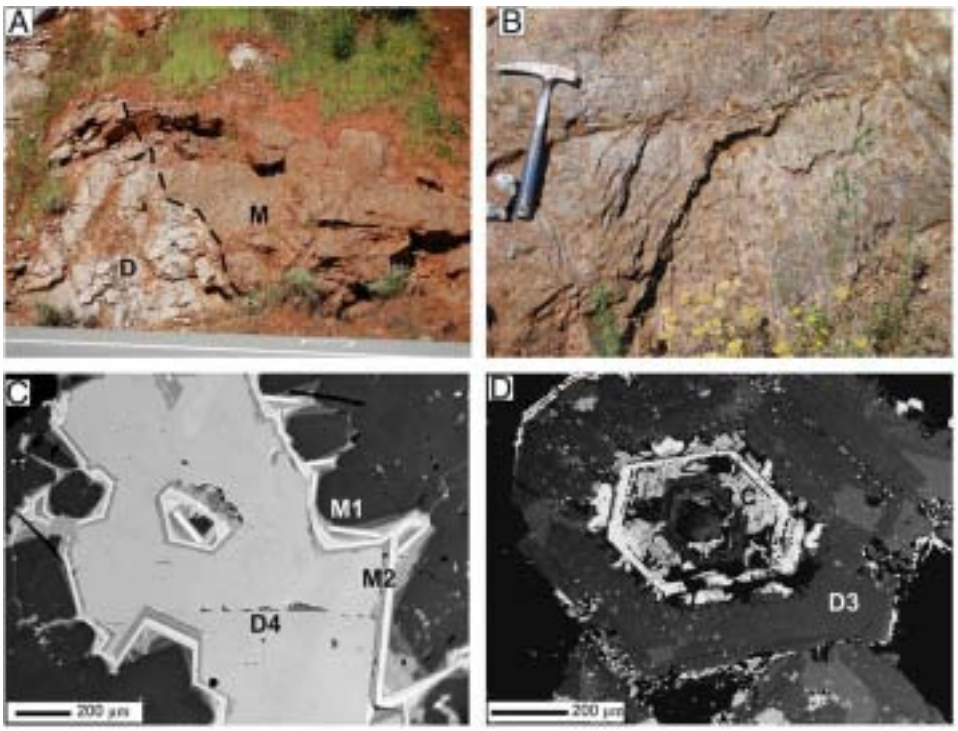

Fig. 6. A) Magnesitization front; magnesite (M) replacing dolostone (D). B) Detail of the boxwork vug pattern generated by pressure release observed in the outcrop. Note the preferential lineation. C) Electron microprobe images of M1 and M2. The lighter color of M2 indicates its higher Fe content. Dolomite 3 (D3) fills the porosity. D) Magnesite pseudomorphs composed of LMC. (C) D4 dolomite appears outside the magnesite pseudomorphs.

between MnO or FeO (Fig. 11B, C) and MgO contents. SrO shows wide (0–0.107 wt.%) yet similar variation in the two magnesite phases (Fig. 11D). Under cathodoluminescence, the dolomite and magnesite crystals show a red uniform luminescence. Other authors (Boni et al., 2000) have related this lack of any detectable zoning to the presence of Mn^{2+} and low Fe^{2+} concentrations below 1.5 wt.% and an Fe/Mn ratio <7.5. Calcites are mostly LMC and contain small amounts of MgO (1.37 wt.%) and FeO (1.28 wt.%) (Fig. 9).

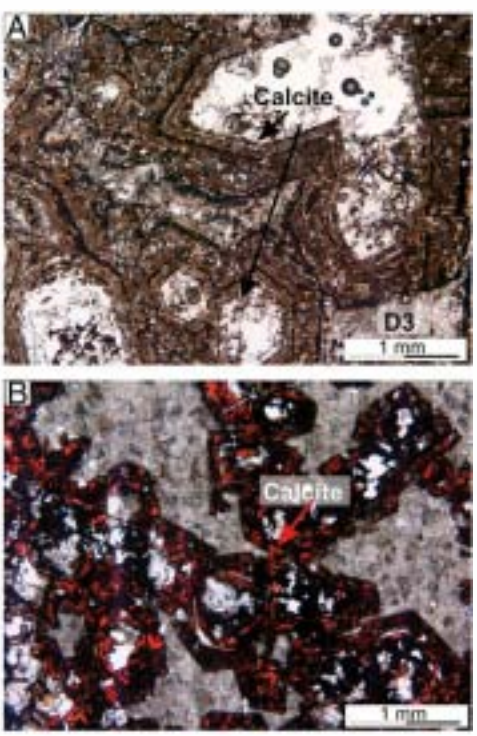

Fig. 7. A) Magnesite pseudomorphs cemented by calcite. Outside the magnesite pseudomorphs D3 dolomite occur. B) Stained thin section showing calcite cemented magnesite pseudomorphs and D3 dolomite.

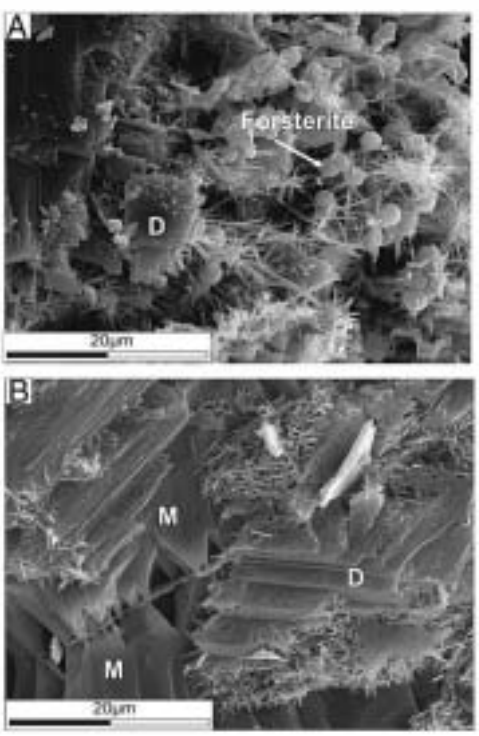

Fig. 8. SEM images. A) Forsterite spheres within pore spaces of the dolomite and magnesite crystals. B) Magnesite crystals (M), dolomite crystals (D), and goethite (G).

Table 1
Summary of electron probe microanalyses (wt.%) of the different carbonate phases.

	CaO	MgO	FeO	SrO	MnO	Mn/Sr
Dolomite 1 and 2 (D1 and D2)						
Media	29.10	21.08	0.98	0.06	0.12	2.39
Standard deviation	0.86	0.44	0.76	0.03	0.12	0.14
Minimum	27.47	20.33	0.04	0.01	0.01	0.14
Maximum	30.54	21.97	2.78	0.13	0.50	8.31
N = number of analyses	20					
Dolomite 3 (D3)						
Media	28.25	20.04	2.01	0.06	0.16	4.04
Standard deviation	4.58	0.98	1.35	0.08	0.11	3.85
Minimum	21.65	17.21	0.05	0.00	0.00	0.00
Maximum	33.00	22.46	5.49	0.50	0.44	15.95
N = number of analyses	54					
Dolomite 4 (D4)						
Media	29.04	20.58	1.65	0.03	0.13	6.40
Standard deviation	0.16	0.31	0.43	0.01	0.06	7.67
Minimum	28.78	20.13	1.07	0.01	0.06	1.53
Maximum	29.24	21.83	2.19	0.04	0.20	20.00
N = number of analyses	5					
Fe-poor magnesites (M1)						
Media	0.20	43.00	3.26	0.04	0.12	6.16
Standard deviation	0.10	0.77	1.18	0.02	0.05	11.25
Minimum	0.04	41.85	1.72	0.01	0.02	0.24
Maximum	0.65	44.31	5.60	0.09	0.25	49.60
N = number of analyses	32					
Fe-rich magnesites (M2)						
Media	0.23	36.04	14.91	0.02	0.64	58.91
Standard deviation	0.15	4.98	6.42	0.03	0.38	77.40
Minimum	0.02	24.41	7.02	0.00	0.01	1.57
Maximum	0.57	41.80	30.63	0.11	1.55	207.33
N = number of analyses	44					
Calcites (C)						
Media	52.71	1.37	1.28	0.03	0.05	2.30
Standard deviation	3.08	1.18	2.10	0.03	0.04	2.32
Minimum	45.89	0.36	0.03	0.00	0.00	0.08
Maximum	56.66	5.10	8.52	0.10	0.14	7.50
N = number of analyses	22					

6.2. $\delta^{18}O$, $\delta^{13}C$ and strontium isotopes of the dolomite and magnesite phases

$\delta^{18}O$ values of the D1 and D2 dolomites were +15.43to +17.51‰ SMOW and $\delta^{13}C$ were −2.53 to −0.13‰ PDB (Fig. 12). $\delta^{18}O$ SMOW values of magnesite were +17.87 to +24.31 SMOW‰ and −3.31 to +3.0‰ for $\delta^{13}C$ PDB, whereas $\delta^{18}O$ SMOW values for the D3 and D4 dolomites ranged from +15.45 to +19.61‰ and −4.4 to +3.21‰ for $\delta^{13}C$ PDB (Fig. 12). These values are in the range of those reported by Kralik et al. (1989) for sparry magnesite samples formed by dolomite replacement and differ from these of magnesites from recent playas and sabkhas (Melezhik et al., 2001). The values recorded for D3 and D4 correspond to those defined by Allan and Wiggins (1993) for dolomites formed under high temperature conditions. One dolomite sample and one magnesite sample have as low $\delta^{13}C$ as −9.43 and −7.01‰ PDB respectively.

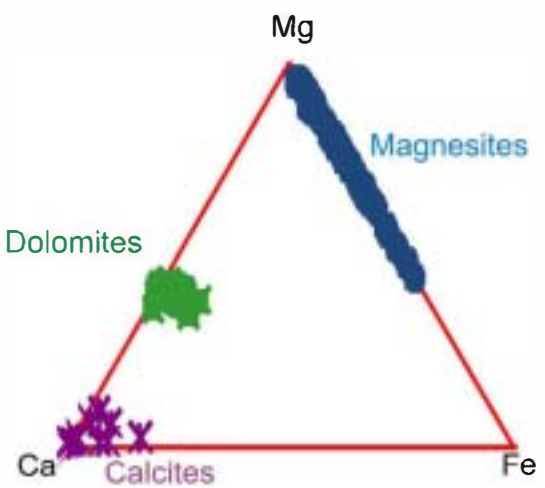

Fig. 9. Plot showing the CaO, MgO and FeO contents of dolomites, calcites and magnesites determined by electron microprobe analyses (wt.%).

Fig. 12 also illustrates the $\delta^{13}C$ isotope values separates the dolomites and magnesites among the three sections. Thus, dolomites and magnesites in the youngest, or Castañar Section, yielded lower $\delta^{13}C$ values when compared with the Robledollano and Navalvillar sections, indicating higher $\delta^{13}C$ with increasing depth and/or age.

Sr isotope values show variations related to the different phases. D1 + D2 dolomites have $^{87}Sr/^{86}Sr$ values of 0.709, D3 + D4 of 0.710 and M1 + M2 show contents that overlap those of the later dolomites D3 and D4 (0.709 to 0.710) (Table 2).

7. Discussion

The critical examination of the different textures observed in the outcrop and thin section analysis and their relationships, along with the geochemical characteristics and isotope compositions permit to establish the sequence of diagenetic events that lead to the formation of the phases previously described (Fig. 13).

7.1. First dolomitization event

The original limestones formed in a mixed siliciclastic–carbonate platform and then underwent dolomitization (Fig. 13). Dolomitization processes only partially preserved the original depositional texture of the parent limestone. This postulation is indicated by replacive phases that mimic previous sedimentary structures and *Cloudina* fossils. D1 and D2 were the result of a replacement process via the circulation of Mg^{2+} bearing solutions, most probably created by progressive evaporation of marine waters within the peritidal environment (sabkha dolomitization model) (Morse and MacKenzie, 1990). Although neither textural nor geochemical evidence evokes a clear dolomitization mechanism, the fact that sedimentary structures are sometimes preserved may indicate a dolomitization process in a not too advanced diagenetic stage. Dolostones seem to be the dominant carbonates within the Precambrian sedimentary record (Tucker and Wright, 1990; Melezhik et al., 2001; Melezhik and Fallick, 2003). The origins of these rocks (sedimentary versus replacement) have been widely disputed (Tucker, 1982), though there are data to suggest that at that time, the physical conditions (T and PCO_2) and Mg^{2+}/Ca^{2+} ratios would promote dolomitization processes whereby preexisting calcite was replaced by dolomite.

$\delta^{18}O$ isotope values for D1 and D2 dolomites are low (+15.43 to +17.51‰ SMOW). In the upper Proterozoic and lower Palaeozoic, the $\delta^{18}O$ signature of marine carbonate material was significantly lower than later on (Allan and Wiggins, 1993). D1 and D2 dolomite phases were probably formed at this time period, where low temperature dolomite acquired this low $\delta^{18}O$ signature during formation. These dolomites were later on partially recrystallized during burial and this might further lowered the $\delta^{18}O$ values (Allan and Wiggins, 1993). The recrystallization is also confirmed by the coarser crystal size of dolomite when it replaces either mud dominated carbonates or grain dominated carbonates. Later recrystallization of these dolostones during burial can cause an increase in crystal size and homogenization of geochemical signatures (Sibley and Gregg, 1987; Morse and Mackenzie, 1990; Moore, 2001).

The $^{87}Sr/^{86}Sr$ ratio of 0.719 obtained here differs from those for the Proterozoic and Lower Cambrian marine carbonates (Burke

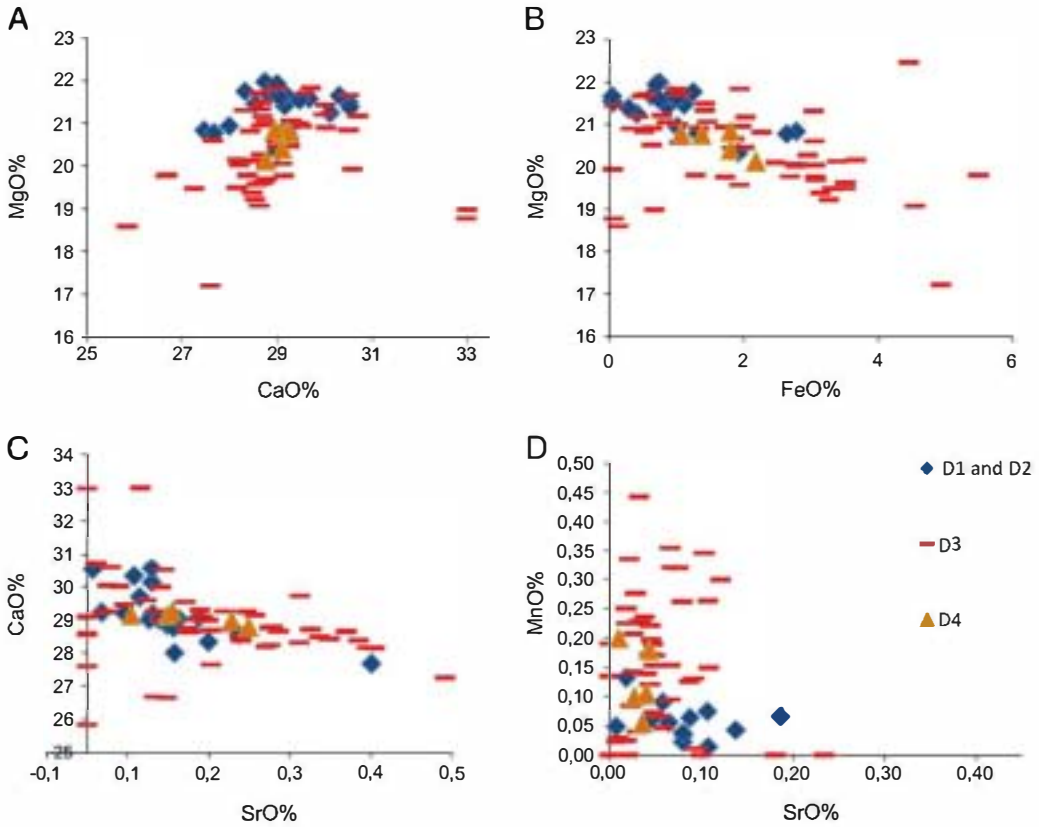

Fig. 10. Geochemistry of the different dolomite phases. A) CaO vs MgO. B) SrO vs MgO. C) SrO vs CaO. D) SrO vs MnO.

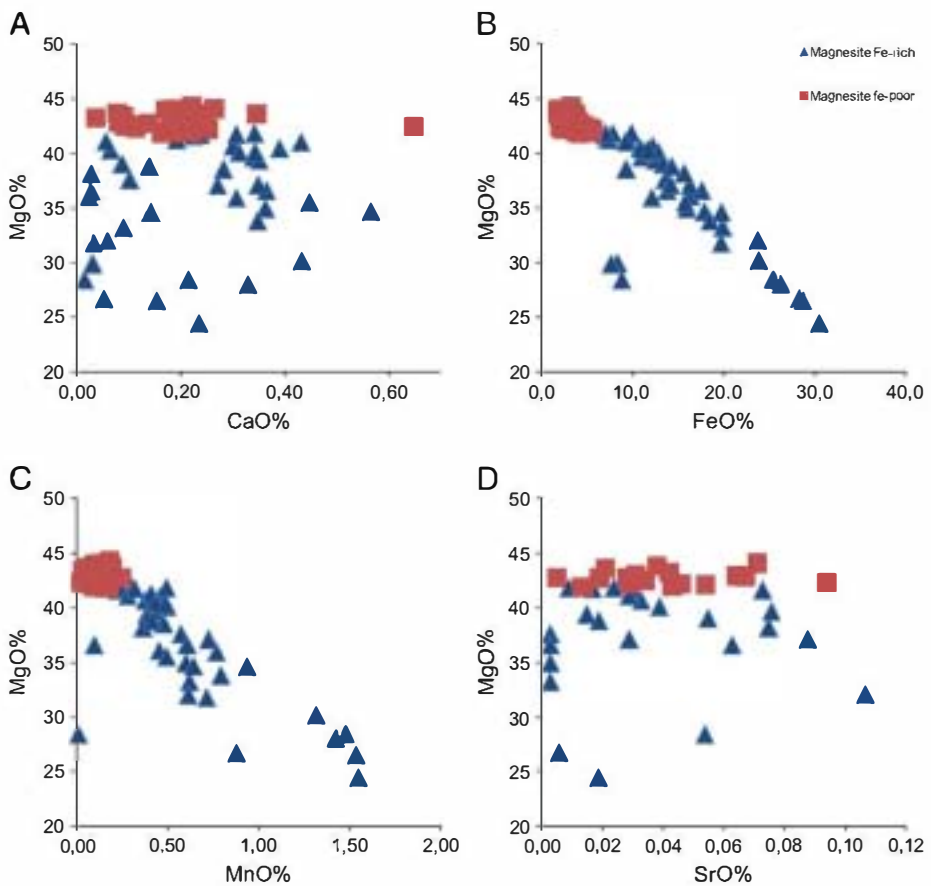

Fig. 11. Geochemistry of the magnesites (M1 and M2). A) CaO vs MgO. B) FeO vs MgO. C) MnO vs MgO. D) SrO vs MgO.

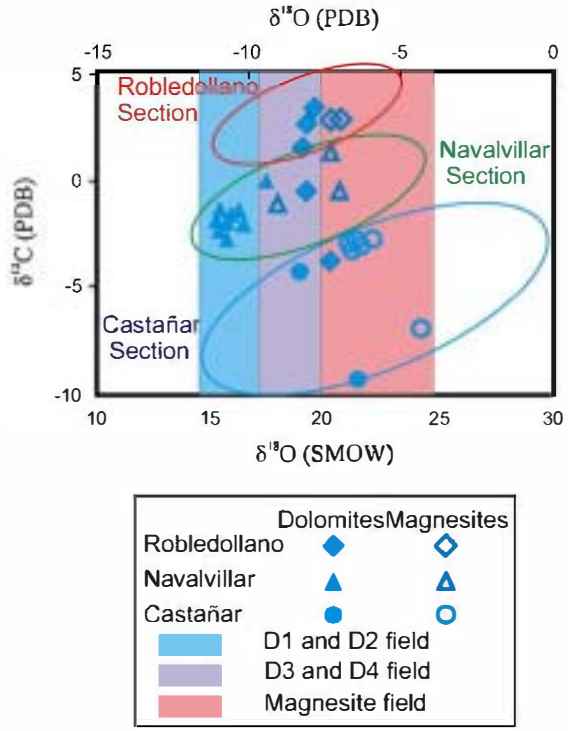

Fig. 12. Covariation plot of $\delta^{13}C$ (PDB) vs $\delta^{18}O$ (PDB) of the dolomites (filled symbols) and magnesites (empty symbols). The three fields correspond to the early dolomite phases (D1 and D2) (most negative $\delta^{18}O$ (PDB) values), the later phases D3 and D4 (high temperature dolomites of Allan and Wiggins, 1993) and the magnesite phases (hydrothermal magnesite $\delta^{18}O$ (PDB) signatures of Kralik et al., 1989).

et al., 1982; Jacobsen and Kaufman, 1999). The presence of stylolites affecting D1 and D2 is an indication of the burial and chemical compaction that these dolostones underwent. Accordingly, this replacement event should represent a burial stage or, as interpreted above, the resetting by recrystallization of initial geochemical signatures.

7.2. Magnesitization event

The main requirements for magnesite formation through dolomite replacement include an increase in the Mg^{2+}/Ca^{2+} ratio and PCO_2. Compaction during burial of the Ibor Group affected siliciclastic deposits, specifically shales, which supplied water enriched in Mg^{2+}. In addition, during diagenesis, fluids enriched in Mg^{2+} may have been formed by Mg-liberating reactions resultant of the formation of chlorites (Fig. 3D) (Morteani et al., 1982; Lugli et al., 2002).This water increased the Mg^{2+}/Ca^{2+} ratio and contributed to magnesite precipitation (Möller, 1989).Experimental work (Franz, 1989) suggests that the stability field of magnesite ranges from very low temperatures and pressures (sedimentary environment) to extremely high temperature conditions (upper mantle). A higher temperature shifts the mineral stability from the dolomite stability field to the magnesite field (Johannes, 1970; Kralik et al., 1989). Hence, processes such as Mg^{2+}-enriched hydrothermal fluid circulation could both enhance Mg^{2+}/Ca^{2+} ratios in fluids and contribute to increase

Table 2
$^{87}Sr/^{86}Sr$ ratios of samples of dolomites and magnesites of the Ibor Group.

Sample	Phase	$^{87}Sr/^{86}Sr$ ratio
ROB-P2	Dolomite (D1)	0.709113
MAG-8	Dolomite (D1)	0.70928
NAV-9	Dolomite (D3)	0.710248
NAV-9	Dolomite (D4)	0.710712
MAG-8	Magnesite (M)	0.709593
TAL-7C	Magnesite (M)	0.710459

temperature conditions (Siegl, 1984). Magnesite appears in outcrop replacing both the dolostones and siliciclastics. The replacement front is appreciable in the field and the textural relationship of the magnesite to fractures, stylolites and bedding planes reveals that the hydrothermal fluids used them as conduits to pass through the rocks (Lugli et al., 2000). The extent and distribution of replacement was controlled by the location of fractures, the nature of the precursor rock and the permeability and the capacity of the solution to pass through (Smith and Davies, 2006).

Magnesite formation is possible at both low and high contents of CO_2 in the fluid phase (Möller, 1989). However, an increase in CO_2 pressure favors the precipitation of magnesite (Möller, 1989) at moderate temperatures. Hydrothermal fluids would increase the CO_2 pressure, similarly to the increase of CO_2 volume produced by metamorphism of calcareous sequences by emplacement of igneous intrusions (Morad, 1998).

The formation of magnesite with iron rich rims (M2), has been explained by Johannes (1970) to be due to retrograde metamorphism. In M2, the decrease in Fe and Mn as the Mg content increases is the outcome of iron and manganese being usually incorporated into the solid phase, whereas magnesium, strontium and barium are preferentially left in the fluid. This leads to a distinct zoning of magnesite, with more Fe-poor cores and Fe-rich rims as temperature decreases (Johannes, 1970). As magnesite precipitates, residual fluids are enriched in calcium.

The stable isotopic composition can be used to further constrain the hydrothermal origin of the magnesite. $\delta^{13}C$ values were −6 to 4.8‰, and $\delta^{18}O$ values higher than −10.6‰ (PDB). Kralik et al. (1989) makes a distinction between magnesites affected by hydrothermal activity and those formed under metamorphic conditions. According to the data provided by Kralik et al. (1989), our values fit in well with magnesites formed during hydrothermal fluid circulation events. The change towards lighter $\delta^{13}C$ values seem to be produced by generation of CO_2 or organic acids generated from the thermal decarboxylation of organic-matter (Davies and Smith, 2006). It could also be modified in response to water–rock interactions or by contributions of oxidized carbon with meteoric waters (Souza et al., 1995). The magnesites of the Ibor Group also show isotope values similar to those found in rocks which have been altered by hydrothermal waters such as those found in mineralizations of cave deposits formed by hydrothermal fluid flows (Bottrell et al., 2001). The studied rocks have undergone several diagenetic events and, thus, isotope values may not correspond to the original isotope values, but rather to those resulting from interactions with later post-depositional fluids.

Magnesites (M1 and M2) are generally more radiogenic than dolomites formed in the first dolomitization event (D1 and D2). Deviations of $^{87}Sr/^{86}Sr$ ratios from that of seawater (Burke et al., 1982; Allan and Wiggins, 1993) could be interpreted as the magnesites being formed by ^{87}Sr enriched fluids. These fluids are commonly related to formation waters which have reacted with siliciclastic sediments with meteoric waters and/or with basement rocks (Veizer, 1989).

Magnesite appears to have formed subsequently to stylolitization of the first dolostones (D1 and D2). At least 500 m of burial is required for stylolite formation in limestones (Fabricius, 2000) (Fig. 13). Brecciation and boxwork vug structures are attributed to hydrofracturing (Davies, 2004; Smith and Davies, 2006) produced when the fluids were expulsed along high permeability faults and fractures into the surrounding strata. The fluids were injected into the sequence, causing brecciation and fracturing of the host rock by pressure release (Smith and Davies, 2006).

7.3. Second dolomitization event and associated processes

The two later dolomite phases (D3 and D4) have a similar chemical and isotope composition, which indicates that they were formed

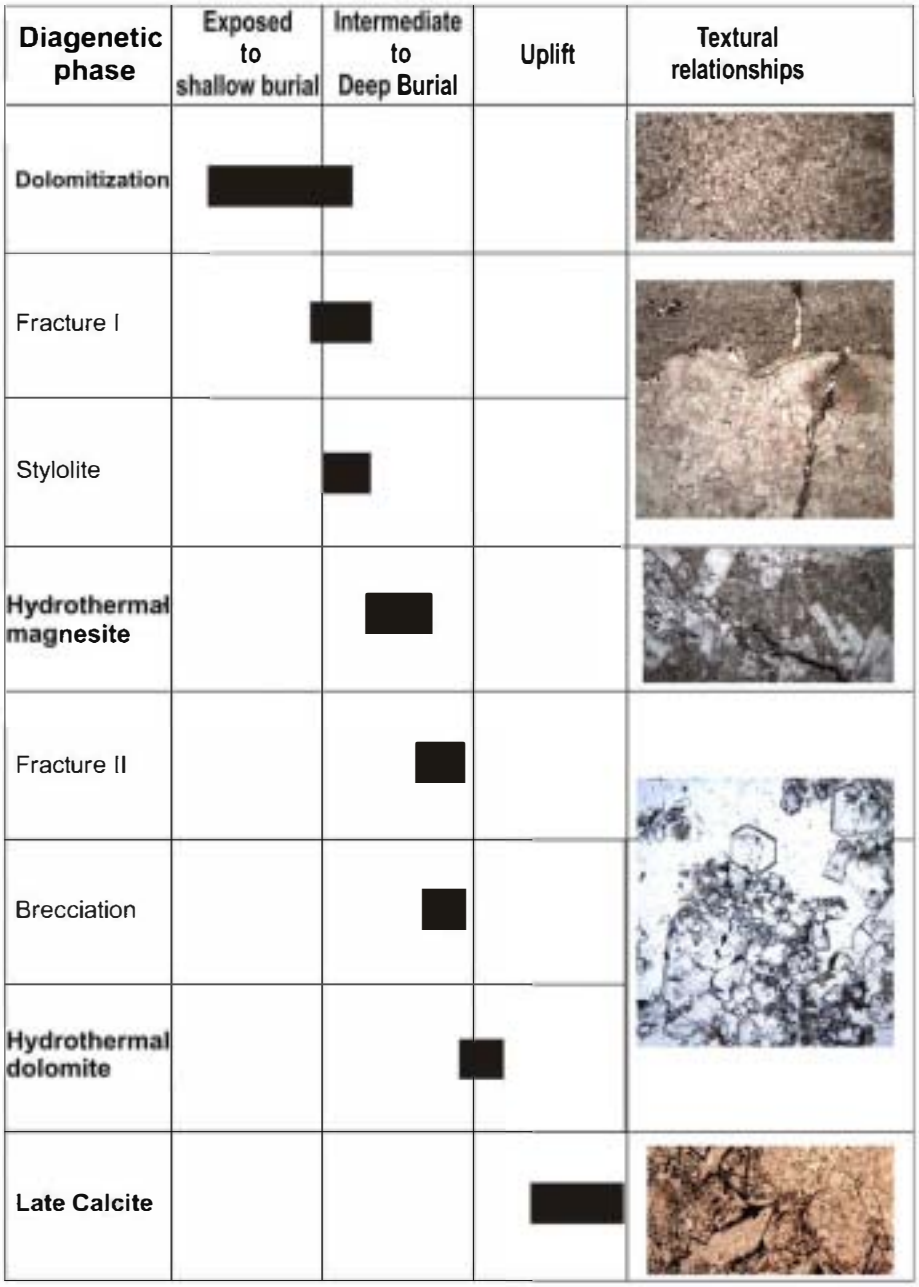

Fig. 13. Diagenetic sequence inferred for the Ibor Group carbonates in the study area. Bars indicate the relative depths of the different diagenetic events. The transition between shallow burial and intermediate-to-deep burial is interpreted as the onset of stylolitization; the transition from burial to uplift is defined by the initiation of the retrograde thermal history.

by a similar fluid and under the same conditions. D3 is a replacive phase whereas D4 is void-filling cement (Fig. 13). Subsequent to magnesite precipitation, the residual fluid became enriched in calcium. Under these conditions, the previous dolomite phases could partially recrystallize to form neomorphic dolomite (D3). In addition, the pores were filled by D4 (dolomite cement). When the pore size is large enough to be appreciable at outcrop scale it is observed that they appear aligned to faults and bedding planes and in close relation to the magnesitization front. Therefore, D4 is interpreted to have been formed postdating the magnesitization event, and that the dolomitizing fluids entered though the rocks using similar pathways. D3 and D4 strontium values appear in the same range of these of the magnesites, and both are enriched in ^{87}Sr compared to D1 and D2. Most burial dolomites on a global scale tend to be enriched in radiogenic ^{87}Sr compared to the inferred strontium composition of ambient seawater (Burke et al., 1982; Veizer, 1989). Enrichment in radiogenic strontium of the later dolomite phases (Table 2) is attributed to the interaction of the formation fluids with siliciclastic or basement rocks rich in Rb-bearing minerals. This same ^{87}Sr enrichment has been found in dolostones formed under hydrothermal conditions (Tornos and Spiro, 2000) and dolomite formed due to magnesite replacement caused by interaction with hydrothermal fluids (Lugli et al., 2000; Kilias et al., 2006).

When comparing the $\delta^{18}O$ isotope values of magnesites and dolostones (Fig. 12) there seems to be fractionation to heavier values from dolostones to magnesites (+18.91‰ to around +19.00‰ respectively). Our results suggest that both dolostones (D3 and D4) and magnesites (M1 and M2) formed under the influence of the same evolving hydrothermal fluids. The fact that dolostones show the lighter values may indicate that most of the dolostones were reset under the

influence of fluids of relatively higher temperature (Allan and Wiggins, 1993).

Fig. 12 shows that $\delta^{13}C$ values also differ in the three sections examined (from 3.21 to −9.43‰ PDB). Thus, light carbon increases from the oldest (deepest) section (Robledollano) to the youngest (Castañar) section. The low $\delta^{13}C$ values recorded for the Castañar section can be interpreted as being the result of a later near-surface weathering (observed in the outcrop) that allowed extended exchange with atmospheric CO_2 at specific pH and PCO_2 conditions (Land, 1980), or due to an increase of CO_2 due to thermal decarboxylation of organic matter (Souza et al., 1995).

Talc appears in joints, fractures and stylolites within the magnesite and later dolomite phases (D3 + D4). The reaction assumed for the main stage of talc mineralization within dolostones is: 3Dolomite + 4Quartz + H_2O = Talc + 3Cc + 3CO_2 (Franz, 1989). The reaction of talc formation from magnesites is: Magnesite + Quartz + H_2O = Talc + CO_2 (Franz, 1989). The latter reaction may even occur at low temperatures (Winkler, 1988). Bucher and Frey (1994) described the formation of talc through decarbonation reactions of magnesite at temperatures lower than 500 °C and from fluids of low PCO_2. The formation of talc from dolomites occurs at temperatures between 300 °C and 400 °C. Therefore, the presence of talc related to D3 and D4 implies that these dolostones underwent temperatures as high as 400 to 500 °C.

The presence of forsterite associated to the magnesite provides additional clues to interpret the interaction of the studied rocks with hydrothermal fluids. Experimental work has shown that by rising total fluid pressure and PCO_2, and decreasing temperature, forsterite can form through the reaction of talc and magnesite (Franz, 1989).

$$\text{Talc} + \text{Magnesite} = \text{Forsterite} + CO_2 + H_2O$$

Dolomite and talc probably formed under the influence of hydrothermal fluid, and the later cooling of this fluid and varying chemical composition led to the formation of forsterite.

7.4. Late calcite cement

Low-Mg calcite appears as a late diagenetic phase (Fig. 13), filling intracrystalline pores, display consistently Fe zoning. This Low-Mg calcite appeared as the rocks were exhumed and subjected to surficial diagenetic processes (Moore, 2001). This idea confirms the inferred oxidation conditions in a meteoric surface environment interpreted for the increase in Fe^{2+} contents (Pierson, 1981). This late stage calcite reduces porosity and permeability in outcrop.

8. Conclusions

The detailed analysis of the magnesite and dolomite phases in the Ibor Group permits to constrain the model of formation and conditions that accounted for their development. Detailed sedimentological, petrographical and geochemical analyses of the carbonate bodies that form part of the Ediacaran Ibor Group succession reveal a complex paragenetic evolution.

Based on facies association analyses and their vertical and lateral stacking pattern, the sequence is interpreted as a mixed siliciclastic–carbonate platform. The age of the succession (between 635 and 542 Ma), has been established based on the appearance of *Cloudina hartmannae* and acritarch fossil remains. These rocks have suffered intense transformations. Dolomite, magnesite and minor traces of talc, forsterite and goethite together with geochemical data and outcrop observations reveal that the principal processes that affected these rocks were related to burial diagenesis and hydrothermal fluid circulation.

Two early dolomite phases (D1 and D2) appear as crystalline replacive dolomite which formed through dolomitization of the original peritidal limestones under evaporate conditions. Crystal sizes variations between D1 and D2 depend on the texture of the precursor limestone. $^{87}Sr/^{86}Sr$ ratios (0.7028 to 0.7091) suggest that recrystallization of these dolostones took place during burial.

Cross-checking stable and Sr isotopes values along with their geochemistry indicate that the magnesites (M1 and M2) were formed through the replacement of D1 and D2 by Mg^{2+} enriched fluids that entered the system via stylolites, fractures and bedding planes. The Mg^{2+} enrichment in the fluid was probably sourced by compaction of lateral detrital sediments and the transformation of clays into chlorites. In addition, possible Mg^{2+} enriched hydrothermal fluids may have contributed to increase both the Mg^{2+}/Ca^{2+} ratio and temperature. The zoning of the magnesite phases into an initial iron-poor phase and a second iron-rich phase reflects variations towards lower temperature conditions of precipitation. Their stable isotope values correspond to those defined by other authors as related to hydrothermal alterations.

D3 and D4 were formed by a similar fluid under similar conditions but D3 replaced D1 and D2, and D4 is a void filling cement. Talc, forsterite and the late dolomites (D3 and D4) formed in relation to hydrothermal fluids as indicated by the stable isotope and $^{87}Sr/^{86}Sr$ of the dolomites. Talc associated with dolomite could have formed through decarbonation of magnesite at temperatures lower than 500 °C. Forsterite formed through the reaction of talc and magnesite, probably as the fluids cooled down.

A late calcite phase appears in some samples replacing magnesite and dolomite phases. This LMC was precipitated during telodiagenesis, when the rocks interacted with surficial fluids of meteoric origin.

Although some questions such as the precise temperature and the mechanisms of circulation of the hydrothermal fluids remain unclear, our study reveals that the occurrence of magnesite deposits within the Ibor Group is the result of complex diagenetic and hydrothermal processes. Both the prior dolostones and the presence of siliciclastic beds suggest an important role for these deposits in the formation of magnesitization fluids. The textural characterization both in the field and in thin section analysis of the magnesites and dolostones as well as their geochemical signatures permits to develop a model of their origin and mechanism of formation that supports the hydrothermal origin of sparry magnesites by replacement of precursor dolostones, similarly to those described in other magnesite deposits like those of Eugui or Rubian deposits in Spain (Lugli et al., 2000; Kilias et al., 2006).

Acknowledgments

This work received financial support from Projects CGL-2008-05584-C02-02 of the MCINN and UCM-910404 of the UCM-CAM and Junta de Extremadura through FEOGA314 ORIENTACION-FEDER funds. B. Jones is thanked for helpful discussion during field work. The manuscript has been improved by the critical comments of S. Morad and P. Pufahl and an anonymous reviewer. R. M-G was supported by a JAEPredoc-CSIC grant and A. M-P by an I3P-CSIC grant. A. Burton carefully reviewed the text.

References

Aharon, P., 1988. A stable-isotope study of magnesites from the Rum Jungle Uranium Field, Australia: implications for the origin of strata-bound massive magnesites. Chemical Geology 69, 127–145.

Al-Husseini, M., Amthor, J.E., Grotzinger, J., Mattner, J., 2003. Arabian Plate Precambrian–Cambrian boundary interpreted in Oman's Ara Group. GeoArabia 8, 578–580.

Allan, J.R., Wiggins, W.D., 1993. Dolomite reservoirs; geochemical techniques for evaluating origin and distribution: AAPG Continuing Education Course Note Series, 36, p. 129.

Alvarez-Nava, H., García Casquero, L., Gil Toja, A., Hernández Urroz, J., Lorenzo Alvarez, S., Lopez Díaz, F., Lopez, M., Monteserin, V., Nozal, F., Pardo, M.V., Picart, J., Robles,

R., Santamaria, J., Solé, F.J., 1988. Unidades lito-estratigráficas de los materiales precámbrico-cámbricos de la mitad suroriental de la Zona Centro-Ibérica. 11. Congr. Geol. Esp., 1. SGE, Granada, pp. 19–22.

Boni, M., Parente, G., Bechstädt, T., De Viro, B., Iannace, A., 2000. Hydrothermal dolomites in SW Sardinia (Italy): evidence for a widespread late Variscan fluid flow event. Sedimentary Geology 131, 181–200.

Bottrell, S.H., Crowley, S., Self, C., 2001. Invasion of a karst aquifer by hydrothermal fluids: evidence from stable isotopic composition of cave mineralization. Geofluids 1, 103–121.

Bucher, M., Frey, M., 1994. Petrogenesis of Metamorphic Rocks. Springer-Verlag, p. 318.

Burke, W.H., Denison, R.E., Hetherington, E.A., Koepnick, R.B., Nelson, H.F., Otto, J.B., 1982. Variation of seawater $^{87}Sr/^{86}Sr$ throughout Phanerozoic time. Geology 10, 516–519.

Cortijo, I., Martí Musa, M., Jensen, S., Palacios, T., 2010. A new species of *Cloudina* from the terminal Ediacaran of Spain. Precambrian Research 176, 1–10.

Craig, H., 1957. Isotopic standards for carbon and oxygen and correction factors for mass spectrometric analysis of carbon dioxide. Geochimica et Cosmochimica Acta 12, 133–149.

Davies, G.R., 2004. Hydrothermal (thermobaric) dolomitization: rock fabric and organic petrology support for emplacement under conditions of thermal transients, shear stress, high pore fluid pressure with abrupt pressure transients, hydrofracturing, episodic rapid fluid flow, and instantaneous cementation by saddle dolomite. In: Davies, G.R., Packard, J., McAuley, R. (Eds.), Dolomite Seminar and Core Conference. Canadian Society of Petroleum Geologists, Calgary, p. 20.

Davies, G.R., Smith, L.B., 2006. Structurally controlled hydrothermal dolomite reservoir facies: an overview. AAPG Bulletin 90, 1641–1690.

Díez-Balda, M.A., Vegas, R., Gonzalez Lodeiro, F., 1990. Part IV Central Iberian Zone. In: Dallmeyer, D., Martinez García, E. (Eds.), Structure. Springer-Verlag, Berlín, pp. 172–188.

Dulski, P., Morteany, G., 1989. Magnesite formation by CO_2 metasomatism during regional metamorphism of the ultrabasic rocks of the Ochsner serpentinite (Zillertaler Alpen, Tyrol, Austria). Monograph Series on Mineral deposits, 28. Borntraeger, Berlin-Stuttgart, pp. 95–104.

Dunn, A.M., Reynols, P.H., Clarke, D.B., Ugidos, J.M., 1998. A comparison of the age and composition of the Shelburne Dyke, Nova Scotia and the Messejana Dyke, Spain. Canadian Journal of Earth Sciences 35, 1110–1115.

Fabricius, I.L., 2000. Interpretation of burial history and rebound from loading experiments and occurrence of microstylolites in mixed sediments of Caribbean sites 999 and 1001. In: Leckie, R.M., Sigurdsson, H., Acton, G.D., Draper, G. (Eds.), Proceedings of the Ocean Drilling Program, scientific results 165: College Station, Texas, Ocean Drilling Program, pp. 177–190.

Franz, G., 1989. Stability of magnesite in carbonate–silicate assemblages; a review. Monograph Series on Mineral deposits, 28. Borntraeger, Berlin-Stuttgart, pp. 259–268.

IGME, 1978. Mapa y memoria explicativa de la Hoja 653 (Valverdeja) del mapa geológico de España a escala 1:50,000 (2ª serie). IGME, Madrid.

IGME, 1983. Mapay memoria explicativa de la Hoja 652 (Jaraicejo) del mapa geológico de España a escala 1:50.000 (2ª serie). IGME, Madrid.

IUGS, 2009. International Stratigraphic Chart. International Commision on Stratigraphy. http://www.stratigraphy.org/2009.

Jacobsen, S.B., Kaufman, A.J., 1999. The Sr, C and O isotopic evolution of Neoproterozoic seawater. Chemical Geology 161, 37–57.

Jarosewich, E., Nelen, J.A., Norberg, J.A., 1980. Reference samples for electron microprobe analysis. Geostandards Newsletter 4, 43–47.

Johannes, W., 1970. Zur entstehung von magnesitvorkommen. Neues Jahrbuch für Mineralogie Abhandlungen 113, 274–325.

Kilias, S.P., Pozo, M., Bustillo, M., Stamatakis, M.G., Calvo, J.P., 2006. Origin of the Rubian carbonate-hosted magnesite deposit, Galicia, NW Spain: mineralogical, REE, fluid inclusion and isotope evidence. Mineralium Deposita 41, 713–733.

Kralik, M., Aharon, P., Schroll, E., Zachmann, D., 1989. Carbon and oxygen isotope systematics of magnesites: a review. In: Moller, P. (Ed.), Magnesite, Monograph Series on Mineral deposits, 28. Berlin-Stuttgart, Borntraeger, pp. 197–224.

Land, L.S., 1980. The isotopic and trace element geochemistry of dolomite: the state of the art. In: Zenger, D.H., Dunham, J.B., Ethington, R.L. (Eds.), Concepts and Models of Dolomitization: SEPM Spec. Publ., 28, pp. 87–110.

Le Guerroué, E., Allen, P.A., Cozzi, A., 2006. Chemostratigraphic and sedimentological framework of the largest negative carbon isotopic excursion in Earth history: the Neoproterozoic Shuram Formation (Nafun Group, Oman). Precambrian Research 146, 68–92.

Liñán, E., Gozalo, R., Palacios, T., Gámez Vintaned, J.A., Ugidos, J.M., Mayoral, E., 2002. Cambrian. In: Gibbons, W., Moreno, T. (Eds.), The Geology of Spain. The Geological Society, London, pp. 17–29.

López-Guijarro, R., Armendáriz, M., Quesada, C., Fernández-Suárez, J., Murphy, J.B., Pin, C., Bellido, F., 2008. Ediacaran–Palaeozoic tectonic evolution of the Ossa Morena and Central Iberian zones (SW Iberia) as revealed by Sm–Nd isotope systematics. Tectonophysics 461, 202–214.

Lotze, F., 1956. Das Präkambrium Spaniens. Neues Jahrbuch für Geologie und Paläontologie, Monatshefte 8, 373–380.

Lugli, S., Torres-Ruiz, J., Garuti, G., Olmedo, F., 2000. Petrography and geochemistry of the Eugui magnesite deposit (Western Pyrenees, Spain): evidence for the development of a peculiar zebra banding by dolomite replacement. Economic Geology 95, 1775–1791.

Lugli, S., Morteani, G., Blamart, D., 2002. Petrographic, REE, fluid inclusion and stable isotope study of magnesite from the Upper Triassic Burano Evaporites (Secchia Valley, northern Apennines): contributions from sedimentary, hydrothermal and metasomatic sources. Mineral Deposits 37, 480–494.

Machel, H.G., Lonnee, J., 2002. Hydrothermal dolomite; a product of poor definition and imagination. Sedimentary Geology 152, 163–171.

Melezhik, V.A., Fallick, A.E., 2003. $\delta^{13}C$ and $\delta^{18}O$ variations in primary and secondary carbonate phases: several contrasting examples from Palaeoproterozoic ^{13}C–rich dolostones. Chemical Geology 201, 213–228.

Melezhik, V.A., Fallick, A.E., Medvedev, P.V., Makarikhin, V.V., 2001. Palaeoproterozoic magnesite: lithological and isotopic evidence for playa/sabkha environments. Sedimentology 48, 379–397.

Möller, P., 1989. Minor and trace elements in magnesite. In: Moller, P. (Ed.), Magnesite, Monograph Series on Mineral deposits, 28. Berlin–Stuttgart, Borntraeger, pp. 173–196.

Moore, C.H., 2001. Carbonate reservoirs: porosity evolution and diagenesis in a sequence stratigraphic framework. Developments in Sedimentology 55, 444.

Morad, S., 1998. Carbonate cementation in sandstones: distribution patterns and geochemical evolution. In: Morad, S. (Ed.), Carbonate Cementation in Sandstones: Distribution Patterns and Geochemical Evolution: International Association of Sedimentologists Special Publication, 26, pp. 1–26.

Morse, J.V., Mackenzie, F.T., 1990. Geochemistry of sedimentary carbonates. Developments in Sedimentology, 48. Elsevier Scientific Publication Co, New York, p. 696.

Morteani, G., Möller, P., Schley, F., 1982. The rare earth element contents and the origin of the sparry magnesite mineralizations of Tux-Lanersbach, Entachen Alm, Spiessnägel, and Hochfilzen, Austria, and the lacustrine magnesite deposits of Aiani-Kozani, Greece, and Bela Stena, Yugoslavia. Economic Geology 77, 617–631.

Müller, G., Irion, G., Förstner, U., 1972. Formation and diagenesis of inorganic Ca–Mg carbonates in the lacustrine environment. Naturwissenschaften 59, 158–164.

Myrow, P.M., Landing, E., 1992. Mixed siliciclastic–carbonate deposition in a lower Cambrian oxygen-stratified basin, Chapel Island Formation southeastern Newfoundland. Journal of Sedimentary Petrology 62, 455–473.

O'Neil, J.R., Clayton, R.N., Mayeda, T.K., 1969. Oxygen isotope fractionation in divalent metal carbonates. Journal of Chemical Physics 51, 5547–5558.

Ohmoto, H., Rye, R.O., 1979. Isotopes of sulfur and carbon, In: Barnes, H.L. (Ed.), Geochemistry of Hydrothermal Ore Deposits, 2nd ed. Wiley-Interscience, New York, pp. 509–567.

Palacios Medrano, T., 2005. Geología Histórica de Extremadura. En: Patrimonio Geológico de Extremadura. In: Junta de Extremadura (Ed.), Consejería de Industria, Energía y Medio Ambiente. Junta de Extremadura, pp. 35–69.

Pierson, J., 1981. The control of cathodoluminescence in dolomite by iron and manganese. Sedimentology 28, 601–610.

Pohl, W., 1989. Comparative geology of magnesite deposits and occurrences. In: Moller, P. (Ed.), Magnesite, Monograph Series on Mineral deposits, 28. Berlin-Stuttgart, Borntraeger, pp. 1–14.

Pohl, W., 1990. Genesis of magnesite deposits – models and trends. Geologische Rundschau 79, 291–299.

Pueyo, J.J., Inglés, M., 1987. Magnesite formation in recent playa lakes, Los Monegros, Spain. In: Marshall, J.D. (Ed.), Diagenesis of Sedimentary Sequences, Geological Society Special Publication, pp. 119–122.

Quemeneur, J.M., 1974. Les gisement de magnesite du Pays Basque: Cadre geoligique et sedimentologique; genese de la magnesite en milieu sédimentaire. Diss. Univ. Paris VI, Unpublished, pp. 210.

Rodríguez-Alonso, M.D., Peinado, M., López-Plaza, M., Franco, P., Carnicero, A., Gonzalo, J.C., 2004. Neoproterozoic–Cambrian synsedimentary magmatism in the Central Iberian Zone (Spain): geology, petrology and geodynamic significance. International Journal of Earth Sciences 93, 897–920.

Schröder, S., Grotzinger, J.P., Amthor, J.C., Matter, A., 2005. Carbonate deposition and hydrocarbon reservoir development at the Precambrian–Cambrian boundary: the Aran Group in South Oman. Sedimentary Geology 180, 1–28.

Schroll, E., 2002. Genesis of magnesite deposits in the view of isotope geochemistry. Boletim Paranaense de Geociências, UFPR 50, 59–68.

Sheppard, S.M.F., Schwarcz, H.P., 1970. Fractionation of carbón and oxygen isotopes and magnesium between coexisting metamorphic calcite and dolomite. Contributions to Mineralogy and Petrology 26, 161–198.

Sibley, D.F., Gregg, J.M., 1987. Classification of dolomite rock textures. Journal of Sedimentary Petrology 57, 967–975.

Siegl, W., 1984. Reflections on the origin of sparry magnesite deposits. In: Wauschkuhn, A., Kluth, C., Zimmermann, R.A. (Eds.), Syngenesis and Epigenesis in the Formation of Mineral Deposits. Springer-Verlag, Berlin, pp. 177–182.

Smith, L.B., Davies, G.R., 2006. Structurally controlled hydrothermal alteration of carbonate reservoirs: introduction. AAPG Bulletin 90, 1635–1640.

Souza, R.S., De Ros, L.F., Morad, S., 1995. Dolomite diagenesis and porosity preservation in lithic reservoirs, Carmópolis Member, Sergipe–Alagoas Basin, Northeastern Brazil. Bulletin of the American Association of Petroleum Geologists 79, 725–748.

Tornos, F., Spiro, B.F., 2000. The geology and isotope geochemistry of the talc deposits of Puebla de Lillo (Cantabrian Zone, Northern Spain). Economic Geology 95, 277–1296.

Tucker, M.E., 1982. Precambrian dolomites: petrography and isotopic evidence that they differ from Phanerozoic dolomites. Geology 10, 7–12.

Tucker, M.E., Wright, P., 1990. Carbonate Sedimentology. Blackwell Scientific Publications, London, p. 482.

Valladares, I., Ugidos, J.M., Recio, C., 1993. Criterios geoquímicos de correlación y posible area fuente de las pelitas del Precámbrico superior-Cámbrico inferior de la Zona Centro-Ibérica (Macizo Ibérico, España). Revista de la Sociedad Geológica de España 6, 37–45.

Valladares, M.I., Barba, P., Ugidos, J.M., Colmenero, J.R., Armenteros, I., 2000. Upper Neoproterozoic–Lower Cambrian sedimentary successions in the Central Iberian Zone (Spain): sequence stratigraphy, petrology and chemostratigraphy: implication for the other European zones. International Journal of Earth Sciences 89, 2–20.

Valladares, M.I., Barba, P., Ugidos, J.M., 2002. Precambrian. In: Gibbons, W., Moreno, T. (Eds.), The Geology of Spain. Geol Soc London, pp. 7–16.
Veizer, J., 1989. Strontium isotopes in seawater through time. Annual Review of Earth and Planetary Science 17, 141–167.
Vidal, G., Jensen, S., Palacios, T., 1994a. Neoproterozoic (Vendian) ichnofossils from the Lower Alcudian strata in central Spain. Geological Magazine 131, 169–179.
Vidal, G., Palacios, T., Diez Balda, M.A., Gámez Vintaned, J.A., Grant, S.W.F., 1994b. Neoproterozoic–early Cambrian geology and paleontology of Iberia. Geological Magazine 131, 729–765.
Vidal, G., Palacios, T., Moczydlowska, M., Gubanov, A.P., 1999. Age constraints from small shelly fossils on the early Cambrian terminal Cadomian Phase in Iberia. Geologiska Föreningens i Stockholm Förhandlingar 121, 137–143.
Vilas, F., Arche, A., Ferrero, M., Bujalesky, G.G., Isla, F.I., González-Bonorino, G., 1987. Esquema evolutivo de la sedimentación reciente en la Bahía San Sebastian, Tierra del Fuego, Argentina. Thalassas 5, 33–36.
Villamor-Pérez, M.P., 2002. Cinemática terciaria y Cuaternaria de la falla de Alentejo-Plasencia y su influencia en la peligrosidad sísmica del interior de la Península Ibérica. Tesis Doctoral, Univ. Complutense de Madrid, pp. 343.
Villaseca, C., Eugercios, L., Snelling, N., Huertas, M.J., Castellón, T., 1995. Nuevos datos geocronológicos (Rb–Sr, K–Ar) de granitoides hercínicos de la Sierra de Guadarrama. Revista de la Sociedad Geológica de España 8, 129–140.
Walker, R.G., Plint, A.G., 1992. Wave and storm-dominated shallow marine systems. In: Walker, R.G., James, N.P. (Eds.), Facies Models. Response to Sea Level Change, pp. 219–238.
Winkler, H.G.F., 1988. Petrogenesis of Metamorphic Rocks. Narosa Publishing House, New Delhi, p. 348.
Zachmann, D.W., 1989. Mg-carbonate deposits in freshwater environment. In: Moller, P. (Ed.), Magnesite, Monograph Series on Mineral Deposits, 28. Berlin-Stuttgart, Borntraeger, pp. 61–94.
Zachmann, D.W., Johannes, W., 1989. Cryptocrystalline magnesite. In: Moller, P. (Ed.), Magnesite, Monograph Series on Mineral Deposits, 28. Berlin-Stuttgart, Borntraeger, pp. 15–28.